Using Cross-Sectioning and Embedding Techniques to Quantify Proteins and Polysaccharides in a Biologically Fouled Crossflow Membrane

Thesis

Presented in Partial Fulfillment of the Requirements for Honors in Engineering and Honors Research Distinction in Environmental Engineering at The Ohio State University

By

Samuel Timothy Corbin

B.S. Chemical and Biomolecular Engineering

The Ohio State University

2018

Thesis Committee

Linda Weavers, Advisor

James Rathman

Abstract

Some water filtration systems may use membranes to remove particulates, colloids, and ions. However, biofouling, deposition and growth of biomass on membrane surfaces, severely lowers the efficiency of membrane systems. Techniques such as ultrasonic cleaning have been tested to reverse biofouling. In order to understand the mechanisms underpinning membrane cleaning, fouled membrane structural components such as proteins and polysaccharides have been visualized using fluorescent light microscopy. However, the effectiveness of this imaging is reduced for thick biofilms due to attenuation of the light signal caused by biomass. This research applied up-to-date histological methods to image thick biofilms on fouled membranes. This new method used light microscopy to image cross-sectioned and epoxy-embedded stabilized biofilms. Embedding the membrane in an epoxy stabilized it during sectioning to reduce changes to the biofilm and to facilitate sectioning. Application of these new methods resulted in increased depth visualization of proteins and polysaccharides with less attenuation for cross-sectioned and embedded biofouled membranes than current methods. Development of this technique will facilitate future research into antifouling technology by allowing researchers to collect higher-quality data on the effects of cleaning.

Acknowledgments

This research would not have been possible without the guidance, support, and commitment of my research advisor, Dr. Linda Weavers, and graduate research colleague Anton Rosi. As a research advisor Dr. Weavers invested considerable time and support to developing not only my technical skills, but my skills of thinking critically and with an investigative mindset. She was also invaluable in guiding my work in the face of countless unknowns, and her support was paramount to the success of this research. Anton also made this work possible as he devoted time and support to growing my skills as a researcher. He was also an integral part of this project as he collected the microscopy images and provided expertise on microscopy interpretation, as well as guidance on biological processes and structures. In addition to countless other ways of their support, both Dr. Weavers and Anton showed their beliefs that I could become a researcher.

I would also like to acknowledge others for support, including fellow CEGE and microbiology researchers that created a community conducive to learning and research, and Judith Krigman and others at The Ohio State Campus Microscopy and Imaging Facility. Finally, I would like to acknowledge the support for this research I received from The Ohio State University College of Engineering Undergraduate Research Scholarship.

Vita

Education

May 2014……Saint Francis de Sales HS, Toledo, OH

August 2018……B.S. Chemical and Biomolecular Engineering, The Ohio State University

Fields of Study

Major Field: Chemical and Biomolecular Engineering

Honors Research Distinction: Environmental Engineering

Table of Contents

List of Tables

List of Figures

Chapter 1. Introduction and Background

Increasingly, water purification and wastewater treatment facilities use membrane technology to remove suspended particulates, colloids, and ions. Membranes are highly selective and generate less sludge than standard wastewater activated sludge treatment technologies, such as secondary clarifiers and sand filters [1]. However, throughput and cost-effectiveness of membrane technologies are lowered by decreases in water permeation due to membrane fouling [2]. The most problematic form of fouling has been identified as membrane biofouling, the deposition and growth of bacteria and flocs on the membrane surface [3], [4].

1.1 Biofouling Properties and Structure

Once bacteria have deposited onto the membrane surface, a structure known as a biofilm is formed. This structure is formed through microbial secretions of proteins, polysaccharides and extracellular DNA. The bacterial and microorganism colonies grow and are bound through adhesion and cohesion facilitated by extracellular polymeric substances (EPS), a gel-like biopolymer matrix [3]. The distribution of proteins and polysaccharides on the fouled membrane surface is related to EPS properties, as Metzger et al. [5] discussed when analyzing distinct layers from fouled membranes. Critically, the properties of these structural components relate to the mechanical properties of biofilms, including their resistance to cleaning.

Studies of biofilm structure from membrane fouling also included information about the amounts of proteins and polysaccharides present. These amounts vary in structure, such as a higher ratio of polysaccharides to proteins on the top layer of the fouling [6]. The different distribution of polysaccharide and protein components in biofilm structures also affected cleaning factors. Yun et al. [7] suggested that the cohesive and adhesive forces of EPS held the biofilm matrix together, and the spatial distribution of biofilm components affected cleaning mechanisms. In addition, thin layers of polysaccharides on the membrane surface that initially attached provided sites for more biofouling attachment and growth [8].

Fouling structure also influenced biofilm removal mechanisms. Structures such as different stratified layers in the biofilm had different resistances to mechanical stress [9]. Walter et al. [9] observed three stratified layers of biofilms: a top layer that was the weakest and accounted for 60% of the detachment of the initial biomass, an intermediate layer that was stronger, and the deepest layer at the membrane surface that was the strongest. These different stratified layers were affected by removal mechanisms such as erosion and sloughing, or shedding of cells from the biofilm. There is also research on how the shape of biofilms may affect removal. Chambless and Stewart [10] created biofouling simulations where the deeper initial fouling layers lost nutrients due to growth of layers above them. These lower layers would die and create mushroom-shaped biofilms with large fouling concentrations at the top, which were more susceptible to sloughing due to breakage of the thinner supporting necks [10].

1.2 Biofouled Membrane Cleaning Technologies

Current techniques to remove biofouling from membranes include mechanical removal such as backwashing, and chemical removal such as chlorine and citric acid [11]. However, these cleaning techniques have several drawbacks. Both techniques create process downtimes of up to 12.6 hours per week for intermittent backwashing, and 4 hours per week for chemical cleaning [12]. In addition, backwashing increases mechanical stress on the membranes. Also, chemical cleaning may not kill all the bacteria and causes releases of EPS that further reduce flow [3]. The drawbacks of these cleaning techniques cause reduced process throughput, increased operating and maintenance costs, and reduced membrane lifetimes. Therefore, research into alternative cleaning techniques is needed to improve these membrane processes.

Alternative membrane cleaning technologies such as ultrasonic cleaning and piezoelectric membranes can improve foulant removal and reduce cleaning time, improving system efficiency [13]. One mechanism for ultrasonic cleaning is cavitation caused by the alternating compression and rarefaction from ultrasonic waves near the membrane surface. Piezoelectric membranes, which are made of electrically poled ceramic materials, produce ultrasonic frequency vibrations when electrically excited [14]. This is a particularly promising technology because piezoelectric membranes may overcome scale-up issues of ultrasonic cleaning caused by the co-location of the ultrasound source to the biofouling. However, it is unclear how the mechanism of biofilm binding affects piezoelectric membrane cleaning. Therefore, research analyzing

membrane biofouling structure and growth provides insight into effective design of these alternative cleaning techniques.

1.3 Confocal Laser Microscopy Use and Limitations

The structure and components of biofilms may be visualized using optical sectioning by confocal laser scanning microscopy (CLSM), a technique that distinguishes different biofilm components based on fluorescent emission [15]. CLSM operates by shining an excitation laser onto a sample and observing the fluorescent emission that is reflected back through a dichroic mirror (see Figure 1 for schematic). The emission

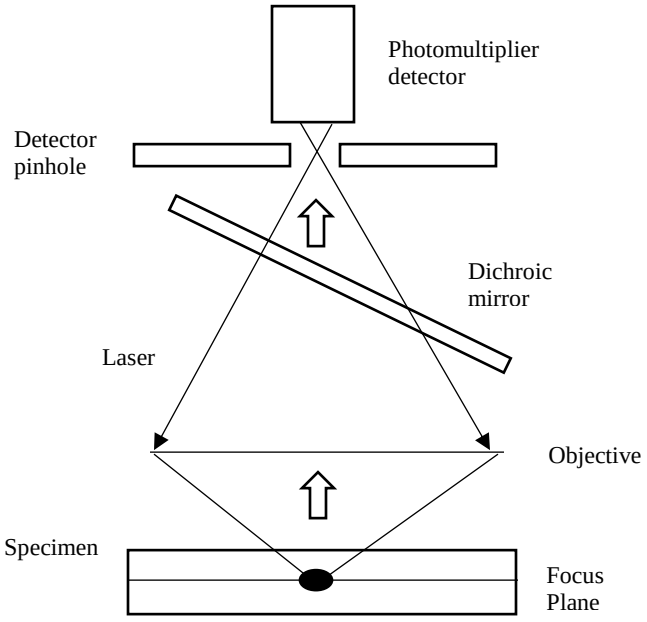

Figure 1: Schematic image of confocal laser microscopy operation, adapted from Ferrando et al. [15]. This image highlights the ability of CLSM to gather signal from only one focal plane.

beam passes through a pinhole that excludes light except from one focal plane, allowing the images to go slice by slice through the depth, known as z-slices, to create a 3D image. Depth measurements are advantageous to analyze thin biofilms without modifying their environment [15]. However, optical sectioning techniques for biofouled membranes cannot capture the total depth of thick biofilm structures. Thick biofilms may scatter and absorb the light signal before it is detected, resulting in signal loss [16].

1.4 Embedding and Cross-Sectioning Techniques

Cutting the biofilm and imaging a cross-section is one method of resolving signal loss issues (see conceptual schematic Figure 2). This process, known as sectioning, uses a cutting instrument to cut cross-sections of the membrane. Sectioned membranes are embedded in an epoxy for solidification [17]. This helps prevent damage to the biofilm structure during the sectioning process [18].

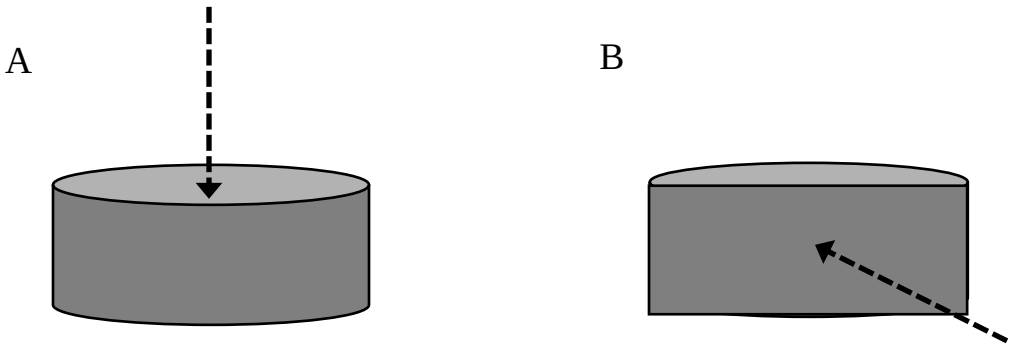

Figure 2: (A) Representation of a fouled ceramic filtration membrane (B) A cross-sectioned fouled membrane. Dashed arrows represent incident beams of light from microscopy.

There have been previous studies of membrane biofilm morphology and possibilities for overcoming limitations of optical sectioning. Chen et al. [19] performed cross-sectioning of frozen, biofouled membranes using a cyromicrotome and analysis by optical imaging. Stabilizing the biofouled membrane by embedding has been used to maintain structure during analysis [18]. The fouled membrane was solidified after embedding which improved sectioning accuracy and prevented biofilm loss and alteration. Xue et al. [20] tested fouled membrane CLSM imaging alteration parameters, including staining samples with fluorophores and storage. Changing such parameters showed that lack of stabilization during sample preparation caused error in measurements of biofilm thickness. This alteration of the biofilm highlighted the need for coupling the sectioning and stabilization by embedding.

Chapter 2. Objective

Applying cross-sectioning and epoxy-embedding techniques with biofouled membranes for CLSM imaging has not been utilized before. This study aims to evaluate and test this combined technique to reveal the protein and polysaccharide biofouling structures throughout the entire depth of biofouled and ultrasonically-cleaned membranes. Using fluorescence microscopy and image analysis, I will demonstrate this technique by measuring the biofilm depth distributions on thick membranes. Previously, attenuation of CLSM signals from thick biofilms created skewed depth distributions that appeared to show the biofilm structure disappearing when the depth increased. Improving this analysis technique is key to applying biofilm morphology and cleaning comparisons to different engineered biosystems for water and wastewater treatment.

Chapter 3. Methodology

3.1 Wastewater Samples

Mixed liquor wastewater samples were obtained from the Jackson Pike Wastewater Treatment Plant in Columbus, OH. The samples were stored in a sealed reactor at 7 ˚C. Reactor conditions such as pH, conductivity, dissolved oxygen (DO), total organic content (TOC), and total nitrogen (TN) were measured (see Table 3, Appendix C). These measurements were used to ensure consistent wastewater sample qualities during testing.

3.2 Crossflow Module and Membrane Fouling

A crossflow membrane module, commonly used in membrane reactor systems, was used for fouling experiments. This apparatus operated by circulating wastewater across the membrane surfaces, causing permeate to flow perpendicular to the wastewater flow. The membrane module contained 4 positions for 25 mm radius Whatman Anodisc ceramic membranes (GE Healthcare Life Sciences, Marlborough, MA). The membranes were connected to a vacuum pump system to provide vacuum-induced permeation. The membrane surface of optical section membranes was marked using a fluorescent marker so it would appear during CLSM. Fluid flow through the module was provided by a MasterFlex peristaltic pump (Cole-Parmer, Vernon Hills, IL). A schematic of the fouling setup is shown in Figure 3.

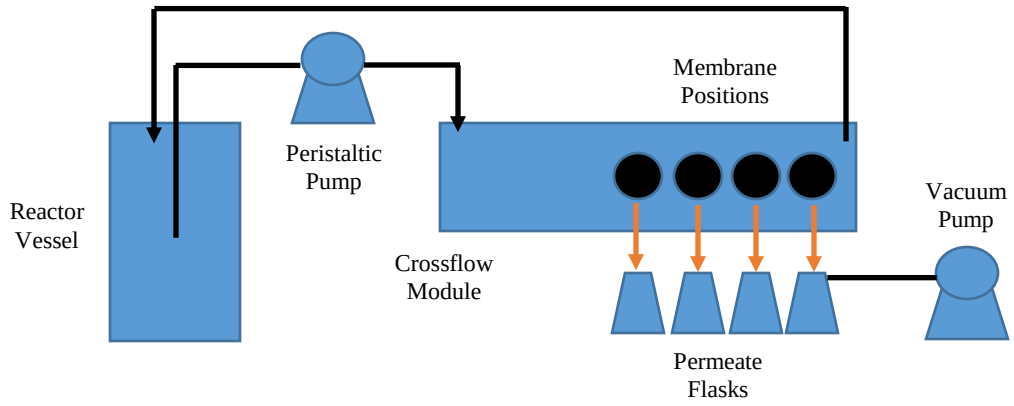

Figure 3: Crossflow fouling flow schematic. Black lines represent wastewater flow, and orange lines represent membrane permeate flow.

Membrane fouling consisted of an initial fluid flow test using de-ionized (DI) water, followed by fouling using a wastewater flow. The initial DI water flow test ensured the vacuum filtration was consistent among the membrane positions and that no membranes were broken. Membrane fouling required approximately two liters of wastewater from a water-jacketed storage reactor to circulate through the crossflow module. The wastewater was kept at a constant temperature of 20 ˚C, 20 L/min aeration rate, and medium agitation. The applied vacuum pressure was approximately 400 mbar, and the wastewater flowrate was approximately 10 mL/sec. Fouling occurred for approximately twenty-four hours.

3.3 Ultrasound Reactor

An ultrasound reactor (L-3 Communications: ELAC Nautik, Kiel, Germany) was used to sonicate specified fouled membrane samples. The reactor was connected to a Cesar power generator (ELAC, Fort Collins, CO) and was set at a frequency of 205.5 kHz and a power of 150 W. Selected samples were placed in the reactor vessel filled

with 1X PBS, and oriented with the fouled membrane facing down toward the transducer. These samples were subjected to 20 seconds of sonication treatment, and then removed from the reactor.

3.4 Fluorescent Staining

Following fouling, fluorescent stains were used to mark protein and polysaccharide components for microscopy analysis. A concentration of 200 μg/mL Alexa Fluor 633 Conjugated Concanavalin A (ThermoFisher Scientific, Waltham, MA) marked polysaccharide components, and a concentration of 8 μg/mL Cascade Blue acetyl azide trisodium (ThermoFisher Scientific, Waltham, MA) marked protein components. The fouled membrane in the first position of the module was cut into three pieces to provide autofluorescence and stain validation controls. The remaining three fouled membranes were all stained with 400 μL of Cascade Blue, followed by three rinses with 400 μL of phosphate-buffered saline (PBS) solution. Then they were subsequently stained with 400 μL of Alexa 633, followed by two rinses with 400 μL of PBS.

3.5 Membrane Embedding and Sectioning

Stained membranes were first fixated in a graded ethanol series, which stopped all biological processes in the biofilms. The ethanol series increased in ethanol concentration from 70% to 100% with samples treated for 4 minutes in each series concentration. The ethanol also dehydrated the biofouled membranes before they were embedded in a hygroscopic epoxy. The epoxy mixture (Sigma-Aldrich, St. Louis, MO) was prepared according to the specified kit instructions [21]. Approximately 0.16 grams of epoxy accelerator was added to the epoxy mixture to give the embedded membranes

the optimum hardness for sectioning. After the epoxy mixture was made the dehydrated membranes were placed in a series of fresh epoxy mixtures, and then placed in aluminum foil holders and covered with 1-2 mL of epoxy mixture. The epoxy covered membranes were cured in an oven at 100 ˚C for one hour, and stored in a – 4 ˚C freezer before sectioning. The samples were stored in the freezer to preserve the stains, and because time restraints required imaging to be performed up to two days later. The samples were sectioned before imaging.

Before sectioning, the samples were removed from the freezer and placed in the oven at 100 ˚C for one minute to make them pliable. Samples were sectioned by first cutting the sample into four quadrants with scissors, and then taking thin sections from each quadrant. Approximately six sections were taken for each embedded sample.

3.6 Confocal Microscopy

Microscopy was performed at The Ohio State University Campus Microscopy and Imaging Facility (CMIF). A FE1000 Multiphoton confocal microscope (Olympus Life Sciences, Tokyo, Japan) was used to perform imaging. A 25X water immersion lens was used, and images were collected using three channels including reflectance mode. The channels used excitation laser wavelengths of 405, 488, and 600 nm for Cascade Blue, reflectance, and Alexa 633, respectively. The emission wavelengths that the fluorescent signals were collected at were 420 and 647 nm for Cascade Blue and Alexa 633, respectively. Barrier filters were constant, and changes in laser power were small to reduce nuisance variability on the results. The z-axis depth steps collected, which

represented the distance intervals between depth slices, were 10 micron z steps for optical sections, and 5 micron z steps for embedded sections.

3.7 Image Analysis and Data Processing

Analysis of confocal images was performed using FIJI image analysis software [22]. FIJI was used to extract the depth distribution of protein and polysaccharide data from the images. For embedded cross-sectioned images a z-projection of the series of depth images for proteins and polysaccharides was created. A z-projection compiled all maximum intensity signals from each image in a series of depth images into one image. Next, pixel intensity values with respect to distance were measured. Pixel intensity values represented a semi-quantitative measure of biopolymer concentration. These values were measured along the cross sections of the embedded sections to determine biofilm thickness. In addition, the total membrane biofouling depth was measured, excluding background signal. Also, the mean pixel intensities along the depth of optical sections were measured for thickness information. The resulting data were compiled to describe the spatial distribution of protein and polysaccharide thicknesses for both types of sections. However, the procedure for obtaining depth distributions for optical sections was different than for the embedded sections. The optical section depth distributions were gathered by using a Z-depth profile function in FIJI. This function measured the mean intensity of each image in depth series, rather than raw intensity. Therefore, these differences in data processing between the optical section and embedded section treatments required comparisons using relative intensity values.

To determine the biofouling thickness from biofouling depth distribution data the metric of fouling thickness was used. This metric represented membrane biofouling thickness by incorporating the biopolymer concentrations and total depth measurement of the image. The biopolymer concentrations represented the amount of biofouling growth and attachment, and the length measurements represented the depths of detectable biopolymers. Together these factors provided a thickness estimate of fouling on the membrane. In addition, the pixel intensities in each sample were scaled by the maximum intensity in the sample. This allowed relative intensities to be compared between embedded and optical sections. However, comparisons between sonication treatments of embedded cross-sections used mean thicknesses that were not scaled because the data processing method was the same for these treatments. The relative fouling thickness was calculated using Equation 1. This equation estimated the fouling thickness of each sample as an integral area under the curve of biopolymer concentration vs. depth based on the relative proportion of intensity and the maximum depth measured.

$$Relative\ Thickness = \frac{Mean\ Intensity}{Max\ Intensity} * Total\ Depth \quad (1)$$

3.8 Statistical Analysis

Mean relative fouling thicknesses were compared for significant differences between embedded and optical section treatments. The statistical tests used were two-sample t hypothesis tests for means with unequal variances, and used a significance level of 0.05 (see Appendix A). Statistical test assumptions were that relative fouling

thickness responses followed an approximately normal distribution, the data was randomly sampled, and responses were independent of each other. Variances between treatments were assumed to be unequal because of the variability of biological growth on the membranes. A parametric test was used because the means of the sample data treatments were analyzed and determined to provide the best estimates within the response distributions.

3.9 Experimental Design

Experimental design included measures for control, replication, and randomization. Control treatment groups included controls for each fluorescent stain used, and an autofluorescence control for each experiment trial. Randomization was performed by randomly selecting membrane positions for treatments, with the exception of membrane position one in the crossflow module. This position in the module was damaged and due to time constraints could not be repaired. Therefore fluorescent controls were always used on position one. Randomization was also incorporated into the imaging procedure. Images were taken from random sites on the sections, and sections were randomly chosen from each of the four quadrants that the membrane was divided into. Replication of the entire experiment was performed by using three trials, and replication within each experiment by using treatment replicates. The treatment types and number of samples are listed in Table 1. The section replicates were used to reduce variability in place of membrane replicates because of the time and cost constraints of running many trials. Therefore, when performing statistical tests the sample sizes were set by the number of replicate membranes for each treatment.

Table 1: Experimental sample replicates, treatment types, and section replicates

Trial Number	**Number of Membrane Samples with Treatments**	**Number of Sections per Sample**
1	1 Optically Sectioned, 2 Embedded	6
2	2 Optically Sectioned, 1 Embedded	10
3	1 Embedded with no sonication, 2 Embedded with 20 Second Sonication	6

Chapter 4. Results

4.1 Biofouling Layers Images

FIJI images were used to qualitatively display biofilm formations and structures for the samples. For all images increasing level of brightness corresponded to a higher detection of the protein or polysaccharide components. For embedded cross-sectioned images the membrane was often seen at the bottom of the image as a dim rectangular structure because the membrane lacked fluorescent signal. Protein and polysaccharide structural components of biofilms without sonication treatment for embedded sections are seen in z-projection images in Figure 4. These figures were representative of CLSM results for embedded and cross-sectioned biofouled membranes without sonication.

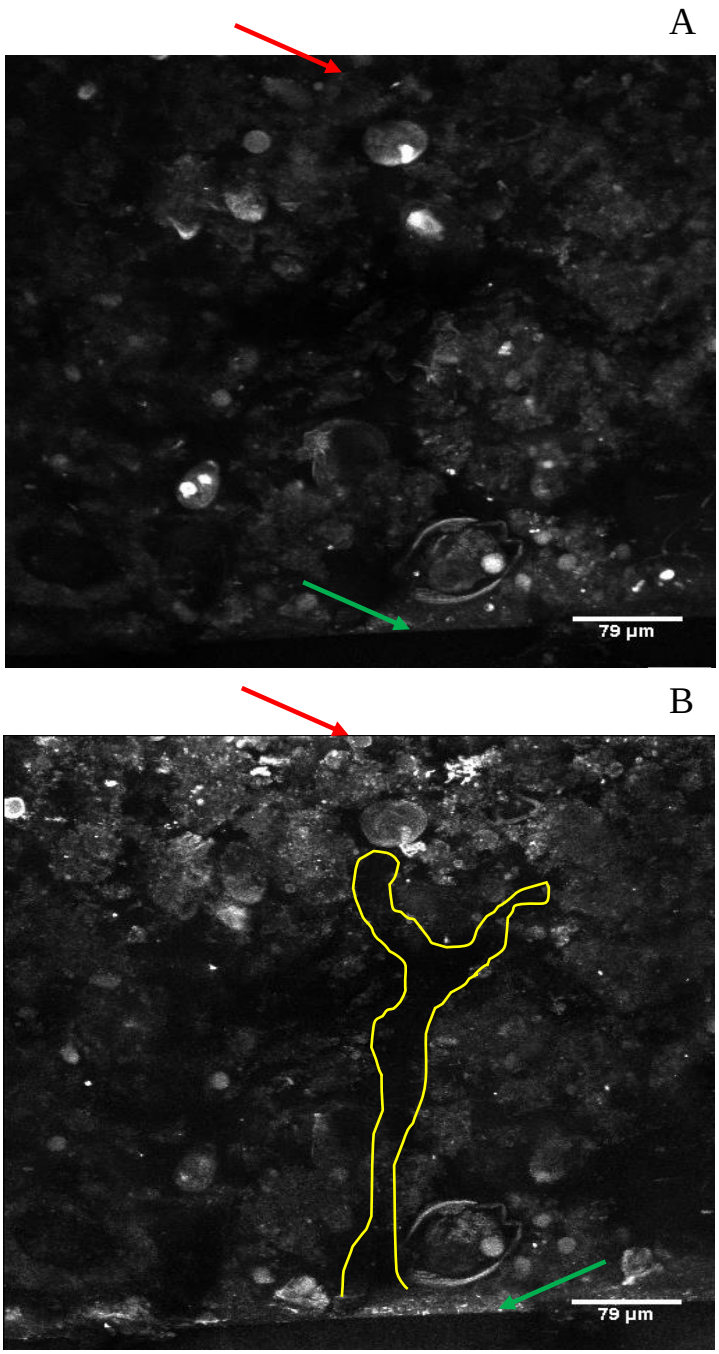

Figure 4: CLSM (A) protein and (B) polysaccharide z-projections of cross-sectioned and embedded membranes. Green arrows identify areas of biofilm attachment to the membrane surface, and red arrows identify the outer-most biofouling layer from the membrane surface. Nutrient flow channels are outlined in yellow.

As shown in Fig. 4A, the protein components of biofilms were growing in several large, globular, high concentration bacterial or microorganism communities dispersed throughout the biofouling layers. On the other hand, the polysaccharide structural components in Fig. 4B included large bacterial or microorganism colonies with high concentrations near the outer layers at the top of the image. These communities were more plume-like colonies and more complex than proteins, representing the matrix of extracellular polysaccharides that biofilms excrete. Moving down from the top of Fig. 4B there were vertical channels that extended to the membrane surface where no polysaccharides were present. These channels represented structures for the transport of nutrients from the top to bottom layers of biofouling, which was consistent with the work of others [10], [19]. There were also high concentration polysaccharide depositions seen at the membrane surface at the bottom of the image. These correspond to the initial biofouling layer attachment and growth.

To highlight differences between optically-sectioned (top views) and embedded cross-sectioned membranes, example optically-sectioned images were prepared. The biofouled membrane polysaccharide and protein structures were analyzed for optical sections and representative 3D-projection images are shown in Figure 5. The optical section z-slices were converted to a 3D image for easier visualization in these figures. In Fig. 5A protein components of colonies were seen in the outer-most fouling layers, but in smaller proportions compared to polysaccharides. Also, note that the large bright spot at the bottom of Fig. 5A was a fluorescent marker that indicated the membrane surface, and not biopolymer signal. Similar structures of high concentration extracellular

A

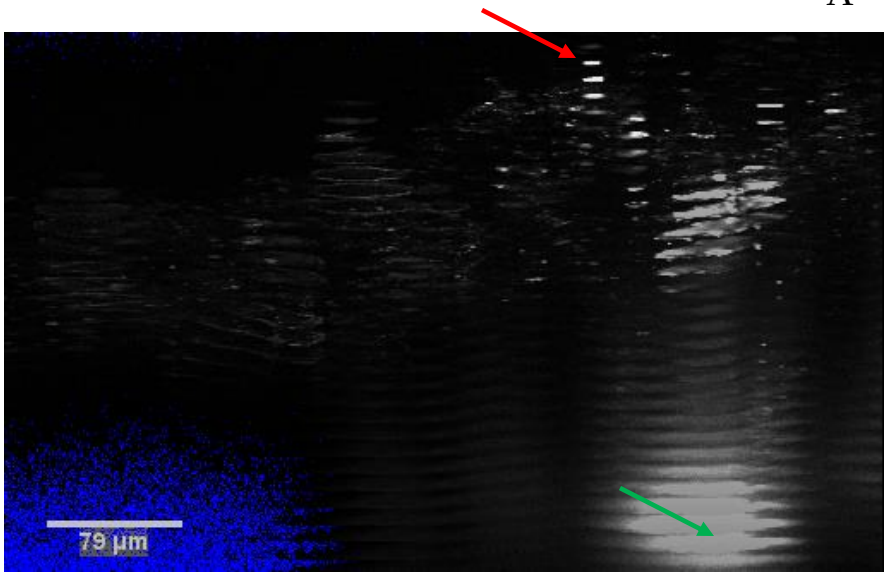

B

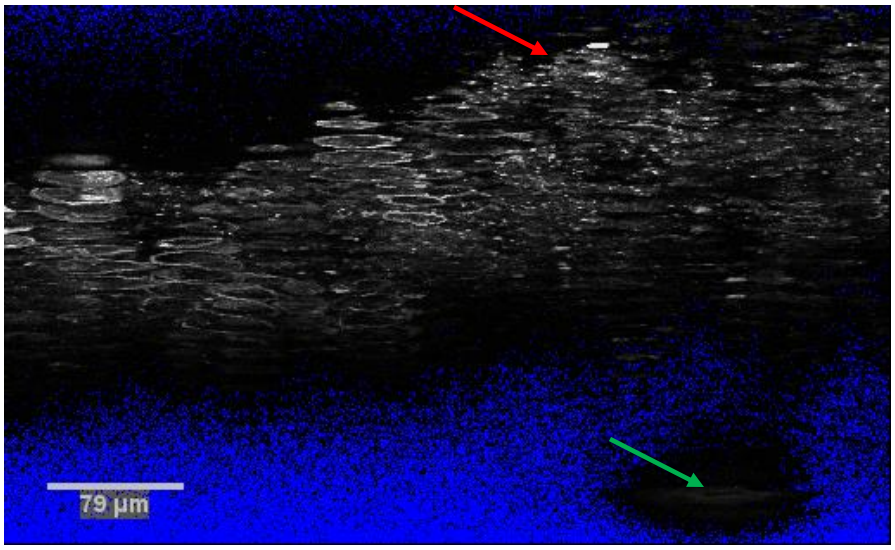

Figure 5: Optical section CLSM 3D-projection image of (A) proteins and (B) polysaccharide biofouled membranes. The green arrow identifies the membrane surface, the red arrow identifies the outer-most biofouling layer from the membrane surface, and the blue areas towards the bottom of the image identify the areas of signal attenuation.

polysaccharides were seen at the top of Fig. 5B, corresponding to the outer-most fouling layer from the membrane surface. However, there was a large area below the outer-most layer that showed no polysaccharide or protein fouling was present, and the initial deposition on the membrane surface was not seen. This discrepancy was due to the attenuation of the light signal in the optically-sectioned images, therefore the layers below the outer-most layer were not able to be quantified. In contrast, the embedded cross-sectioned images revealed interesting features in deeper layers.

Embedded cross-sections were also used to visualize structural fouling components of sonicated membrane samples. Figure 6 shows z-projections of embedded sections from 20 second sonication membrane samples. Fig. 6A showed very low

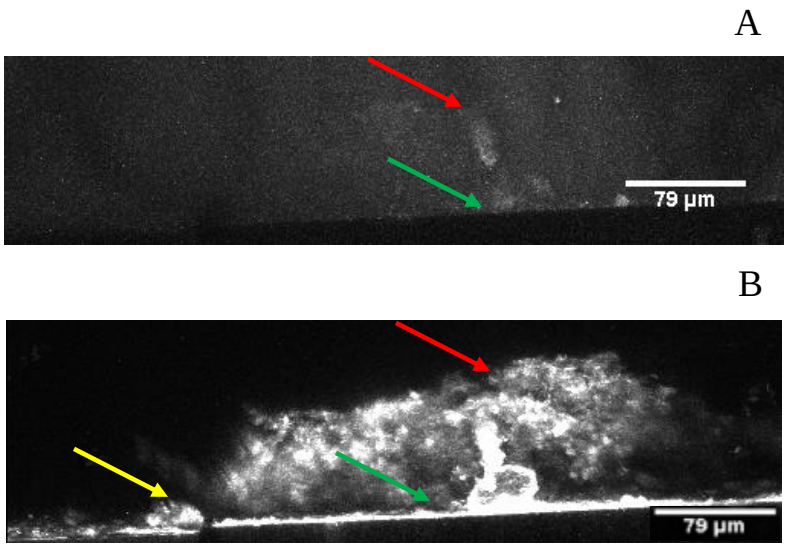

Figure 6: CLSM (A) protein and (B) polysaccharide biofouling z-projections of cross-sections of embedded and sonicated membranes. Green arrows identify areas of biofilm attachment to the membrane surface, and red arrows identify the outer-most biofouling layer from the membrane surface. Yellow arrows identify areas of biofouling removal from the membrane surface due to sloughing from sonication.

protein biofouling concentrations after 20 seconds of sonication. This low protein concentration was due to removal of protein fouling components during sonication. Fig. 6B showed biofouling depth reduction and more concentrated polysaccharide fouling components. This depth reduction was due to the cleaning effects of the ultrasound treatment which included increased sloughing of the top biofouling layer. This was shown by the reduction in total biofouling depth of the sonicated membranes compared to those without sonication treatment (see Table 2, Appendix B). In addition, the biofouling layer did not extend along the entire membrane surface, but was attached in smaller chunks. These results suggested that sonication treatment removed not only the outer-most layers, but layers down to the membrane surface.

4.2 Biofouling Depth Distributions

Confocal microscopy images were analyzed using FIJI image analysis software to quantify information on the thickness of protein and polysaccharide biofouling. The mean protein and polysaccharide biofouling depth distributions for embedded and cross-sectioned membranes without sonication are shown in Figure 7. The data were grouped into sample subsets as an average biopolymer concentration of the sections for each membrane. These distributions showed rising and falling protein and polysaccharide concentrations with biofilm depth, which were related to the stratified regions of growth. Particularly, Fig. 7A showed increased gray value intensity at the membrane surface, approximately 60 μm from the bottom of the images, which indicated a rapid increase in initial protein biofouling. The protein fouling appeared to have high variability, but

A

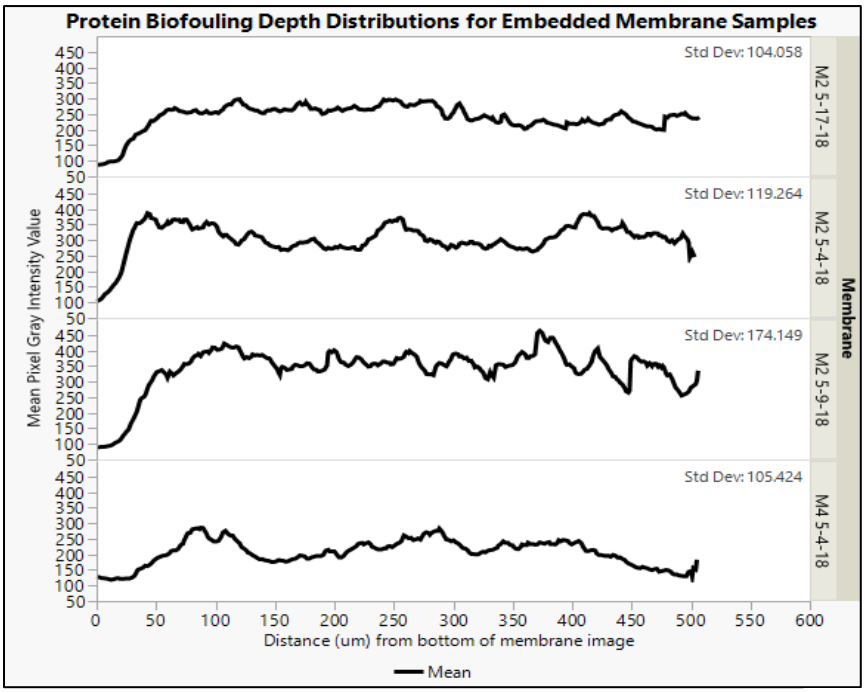

B

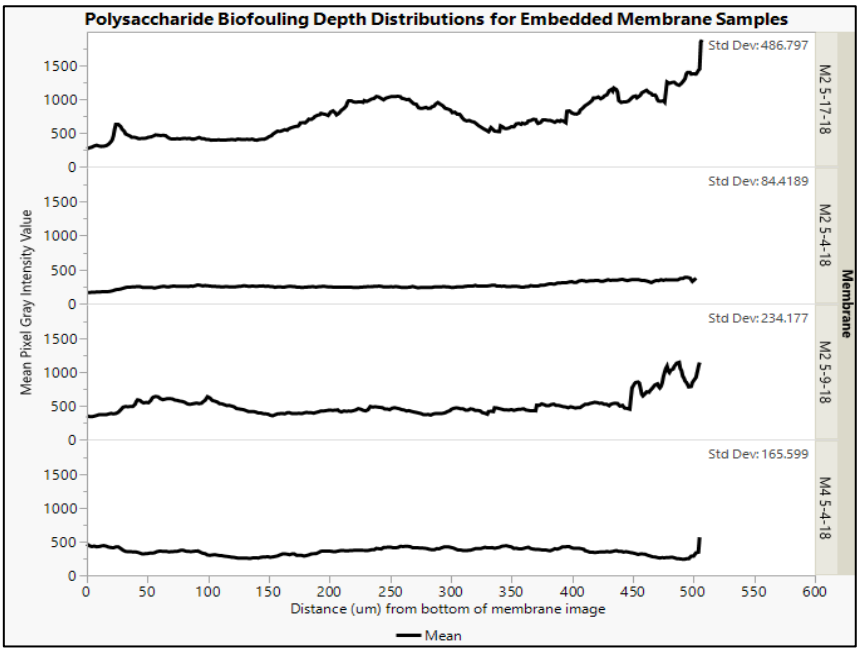

Figure 7: (A) Protein and (B) polysaccharide biofouling concentration depth profiles for embedded and cross-sectioned membranes.

remained relatively stable extending farther from the membrane surface. The polysaccharide biofouling data in Fig. 7B showed increases in the mean biofouling concentration at approximately 400-500 μm from the membrane surface, which corresponded to the outer-most fouling layers. The total biofouling depths measured varied (Table 2, Appendix B), and the maximum depth measured was set by the available viewing width of the microscope, 500 μm. Important trends noted for both proteins and polysaccharide biofouling were that the membranes could be detected by the initial sharp increase in biofouling after a distance of about 60 microns, which corresponded to the thickness of the membrane. Immediately following this at the membrane surface, a sharp biopolymer increase indicated biofilm growth and attachment. The ability to measure this initial fouling layer at the membrane surface was an important validation for use of the embedding and cross-sectioning technique over optical sectioning.

The biofouling depth distributions for the optically sectioned images were also measured. The mean biofouling depth distributions for optically-sectioned proteins and polysaccharides are shown in Figure 8. The distributions in Fig. 8A appeared to show the mean protein biofouling growth and structures increasing as the distance from the membrane surface increased. This low protein biofouling growth near the membrane surface was not seen in the embedded cross-sections, which suggested that this trend may be due to light attenuation. However, the mean polysaccharide depth distributions in Fig. 8B appeared to show a decreasing trend in biofouling extracellular polysaccharide structures as the distance from the membrane surface increased. This suggested that optically-sectioned images displayed a different polysaccharide proportion in outer-most

A

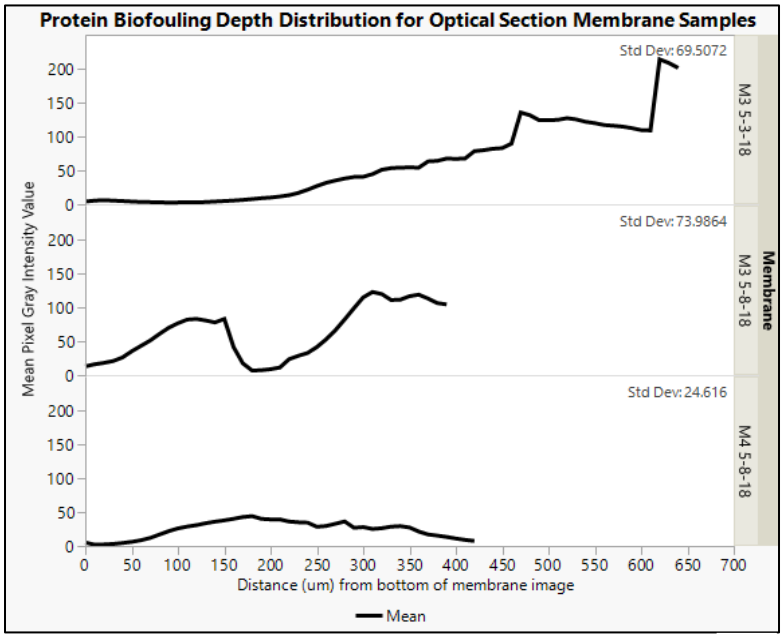

B

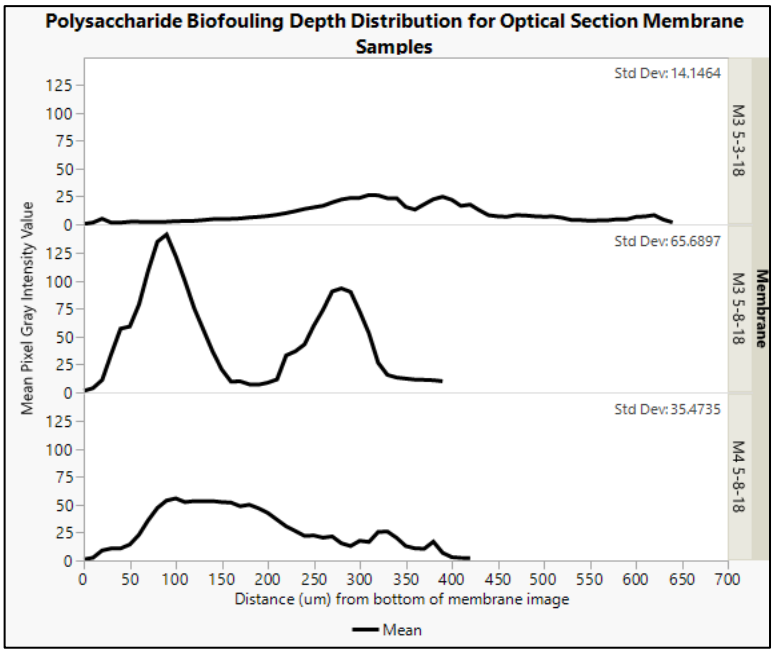

Figure 8: (A) Protein and (B) polysaccharide biofouling concentration depth profiles for optically-sectioned membranes.

layers than embedded sections. This may be due to the degradation of the outer-most fouling layers of optical sections, which were not stabilized in an epoxy. The mean biopolymer concentrations measured for these optical sections were lower than the embedded cross-sections due to differences in FIJI data collection. In addition, the total biofouling depth measured for optically-sectioned images was lower than that measured from embedded sections (see Table 2, Appendix B).

4.3 Biofouling Thickness Comparison

The relative fouling thickness was compared between embedded and optical section samples for polysaccharides and proteins. The embedded sections appeared to capture a larger total biofouling thickness than optical sections. In addition, the embedded cross sections allowed more biopolymer fouling thickness visualization at larger depths than the optical sections. This greater visualization was shown by the increased relative fouling thickness for both proteins and polysaccharides in embedded sections (see Figure 9, Appendix A). This meant that embedded cross-sections not only showed more biofouling at deeper depths, but that the concentration of biopolymers was higher than seen in optical sections. The combination of lower biopolymer concentrations and smaller total depths in optical sections was due to the attenuation of the light signal.

The unscaled biofouling area was used to compare fouling thickness between embedded sections with and without sonication treatment. The protein biofouling thickness was reduced for the embedded membranes with ultrasound treatment (see Figure 10A, Appendix A). This corresponded to removal of the outer-most biofouling

layers and chunks of biofilm from the membrane surface from ultrasound treatment. However, results from the polysaccharide biofouling thickness comparisons suggested that there was not a significant difference between sonication treatments (see Figure 10B, Appendix A). This may have resulted from polysaccharide fouling layers becoming concentrated into small pockets attached to the membrane surface after sonication. These conflicting thickness comparisons may result from the differences in the roles of protein and polysaccharide biopolymers in fouling layers. The polysaccharides may have provided more structural support for the EPS to stabilize the biofilm when a mechanical disruption such as ultrasound was present than the proteins.

Chapter 5. Discussion

5.1 Embedding and Sectioning Technique Evaluation

The embedding and sectioning techniques allowed for biofouled membrane biopolymer structural components to be viewed at all depths without light attenuation. Embedded and sectioned membranes displayed biopolymer components that were not able to be visualized in the optical sections. The embedded sample cross-sections displayed biopolymers at all depths and were not hindered by light attenuation. However, in optical sections light attenuation due to the thick top layer of extracellular polysaccharides obscured visualization of biofouling below it. This attenuation is similar to results from Collier et al. [23] that found that outer-most layers of cells scattered the CLSM light signals from layers below, causing lower concentrations to be measured as the depth increased. Viewing biofouling components at depths near the membrane surface without attenuation gives more information about the initial fouling deposition and growth.

Embedded sections give increased information about the structures and roles of biopolymers on biofouled membranes. The embedded cross-sectioning process allows the stratified layers of the biofouling components to be visualized. These stratified layers include attachment to the membrane surface corresponding to the initial fouling layer, intermediate channels, and the top layer of fouling. The findings are consistent with

other studies of membrane biofouling, which describe an initial fouling layer attachment that then allows mushroom-shaped growth upwards, with channels for nutrient flow [10], [24]. In addition, the differences in stress resistance were seen between the different layers. The outer-most biofouling layer was the most susceptible to removal, as seen in sonication treatments [9]. However, the initial fouling layer was still seen to be attached in both of the sonication treatments. These results are consistent with the findings of Walter et al. [9] that the outer fouling layer was the weakest, while the lowest layer was the strongest. Because these layers are involved with stress resistance and nutrient transport, understanding their locations and structures in biofouled membrane depths is related to mechanisms such as cleaning. However, the locations and concentrations of the intermediate and initial fouling layers are obscured in optical sections. Therefore, the embedded cross-sections show a more promising method for evaluating cleaning procedures such as sonication.

5.2 Sonication Cleaning Treatment

The effects of sonication treatment on biofouling removal and structural changes are able to be visualized by embedding and cross-sectioning biofouled membranes. Comparisons between sonication treatment and untreated fouled membranes for embedded and cross-sectioned membranes displayed the differences in fouling thickness and the remaining biopolymers. This reveals information about the removal processes of the ultrasound treatment. The chunk removal acts as a sloughing mechanism to remove large sections of the biofouling from the membrane. However, the initial fouling layer depositions were still seen. In addition, there were still highly concentrated sections of

polysaccharide biofouling attachment and intermediate layers. Creation of a highly concentrated polysaccharide EPS layer after sonication is consistent with other studies that show biofilms create EPS as a protection from mechanical stress [24]. These findings help interpret how the membranes can be cleaned by sonication, and its viable use as a cleaning method. Because the initial biofouling layer deposition provides the structure and support for growth, disrupting this initial fouling with sonication reduces subsequent growth. Studies have shown this initial layer disruption by sonication to be an effective method of increasing permeate flow and membrane cleaning [11]. In addition, creating more concentrated areas of fouling without nutrient channels may reduce growth rates due to lower nutrient availability and transport.

5.3 Limitations

There were some limitations of the study that impacted the variability of the results. A limited number of membranes were able to be processed due to time and cost constraints, which increased variability between measurements. However, this issue was mitigated by using multiple sections for each sample. While this is not complete replication, clustered sample subsets have been used in other situations where cost can limit sampling [25]. In addition, some CLSM images of the outer-most layers of the embedded sections were limited by the available viewing size of the microscope. In the future, this can be addressed by using an image stitching technique to combine multiple CLSM images into one image to show the entire biofouling distribution.

5.4 Future Research

Membrane biofouling can be continued to be studied with embedding and sectioning techniques in future biofouled membrane cleaning research. Additional studies are needed to analyze the mechanisms underpinning the biofouling depth distributions witnessed from the embedded sections. This includes understanding impacts of different fouling methods, wastewater sources, and membrane technology on the biofilm attachment and structures. These investigations may enable more detailed models to be created that use biofouling depth distributions from the embedded sections to predict structures and layers. This improved structural analysis will allow for detailed inference into how new cleaning methods such as ultrasound can be used effectively in different types of membrane engineered systems.

Chapter 6. Conclusions

The method of embedding and cross-sectioning biofouled membranes for CLSM imaging was more effective for measuring biopolymer structural components at all depths compared to current optical sectioning methods. This new method overcame issues of optical sectioning such as losing biopolymer information at larger depths due to light attenuation in thick biofouled membranes. Embedded cross-sectioned CLSM images allowed visualization of stratified biofouling layers such as the initial layer of deposition and growth, intermediate nutrient flow channels, and the outer-most layer of growth. Embedded images were also used to analyze the effects of ultrasonic cleaning on biofouled membranes, and infer the effects of ultrasonic cleaning during membrane operation. This suggested that ultrasonic cleaning may affect biofouling growth during initial deposition, and increase sloughing removal. However, additional work is needed for analyzing different types of wastewater conditions and membrane fouling systems. Using embedding and cross-sectioning techniques will allow these analyses to create accurate structural models and predictions of cleaning resistances. This information can be used to evaluate new cleaning methods for feasibility and benefits in membrane engineered systems.

References

[1] U.S. Environmental Protection Agency, “Wastewater Management Fact Sheet: Membrane Bioreactors,” pp. 1–9, 2007.

[2] J. Mansouri, S. Harrisson, and V. Chen, “Strategies for controlling biofouling in membrane filtration systems: Challenges and opportunities,” *J. Mater. Chem.*, vol. 20, no. 22, pp. 4567–4586, 2010.

[3] H.-C. Flemming, G. Schaule, T. Griebe, J. Schmitt, and A. Tamachkiarowa, “Biofouling—the Achilles heel of membrane processes,” *Desalination*, vol. 113, no. 2–3, pp. 215–225, 1997.

[4] S. Wang, G. Guillen, and E. M. V Hoek, “Direct observation of microbial adhesion to membranes,” *Environ. Sci. Technol.*, vol. 39, no. 17, pp. 6461–6469, 2005.

[5] U. Metzger, P. Le-Clech, R. M. Stuetz, F. H. Frimmel, and V. Chen, “Characterisation of polymeric fouling in membrane bioreactors and the effect of different filtration modes,” *J. Memb. Sci.*, vol. 301, no. 1–2, pp. 180–189, 2007.

[6] T. Inaba, T. Hori, H. Aizawa, A. Ogata, and H. Habe, “Architecture, component, and microbiome of biofilm involved in the fouling of membrane bioreactors,” *npj Biofilms Microbiomes*, vol. 3, no. 1, 2017.

[7] M. A. Yun, K. M. Yeon, J. S. Park, C. H. Lee, J. Chun, and D. J. Lim, “Characterization of biofilm structure and its effect on membrane permeability in

MBR for dye wastewater treatment," *Water Res.*, vol. 40, no. 1, pp. 45–52, 2006.

[8] F. Meng, S. R. Chae, A. Drews, M. Kraume, H. S. Shin, and F. Yang, "Recent advances in membrane bioreactors (MBRs): Membrane fouling and membrane material," *Water Res.*, vol. 43, no. 6, pp. 1489–1512, 2009.

[9] M. Walter, A. Safari, A. Ivankovic, and E. Casey, "Detachment characteristics of a mixed culture biofilm using particle size analysis," *Chem. Eng. J.*, vol. 228, pp. 1140–1147, 2013.

[10] P. S. Chambless, J.D.;Stewart, "Nanoparticles and microparticles for drug and vaccine delivery.," *J. Anat.*, vol. 189 (Pt 3, no. Ii, pp. 503–505, 1996.

[11] M. Qasim, N. N. Darwish, S. Mhiyo, N. A. Darwish, and N. Hilal, "The use of ultrasound to mitigate membrane fouling in desalination and water treatment," *Desalination*, vol. 443, no. April, pp. 143–164, 2018.

[12] P. Gkotsis, D. Banti, E. Peleka, A. Zouboulis, and P. Samaras, "Fouling Issues in Membrane Bioreactors (MBRs) for Wastewater Treatment: Major Mechanisms, Prevention and Control Strategies," *Processes*, vol. 2, no. 4, pp. 795–866, 2014.

[13] J. K. Krinks, M. Qiu, I. A. Mergos, L. K. Weavers, P. J. Mouser, and H. Verweij, "Piezoceramic membrane with built-in ultrasonic defouling," *J. Memb. Sci.*, vol. 494, pp. 130–135, 2015.

[14] M. T. Darestani, H. G. L. Coster, T. C. Chilcott, S. Fleming, V. Nagarajan, and H. An, "Piezoelectric membranes for separation processes: Fabrication and piezoelectric properties," *J. Memb. Sci.*, vol. 434, pp. 184–192, 2013.

[15] M. Ferrando, A. Rŏzek, M. Zator, F. López, and C. Güell, "An approach to

membrane fouling characterization by confocal scanning laser microscopy," *J. Memb. Sci.*, vol. 250, no. 1–2, pp. 283–293, 2005.

[16] J. M. Vroom *et al.*, "Depth Penetration and Detection of pH Gradients in Biofilms by Two-Photon Excitation Microscopy Depth Penetration and Detection of pH Gradients in Biofilms by Two-Photon Excitation Microscopy," vol. 65, no. 8, pp. 3502–3511, 1999.

[17] P. Baum, M.M. ; Gunawardana, M. ; Webster, "Experimental Approaches to Investigating the Vaginal Biofilm Microbiome," in *Microbial Biofilms: Methods and Protocols*, G. Donelli, Ed. New York, NY: Springer, 2014, pp. 85–103.

[18] J. J. Ganczarczyk, W. M. Zahid, and D. H. Li, "Physical stabilization and embedding of microbial aggregates for light microscopy studies," *Water Res.*, vol. 26, no. 12, pp. 1695–1699, 1992.

[19] M. Y. Chen, D. J. Lee, Z. Yang, X. F. Peng, and J. Y. Lai, "Fluorecent staining for study of extracellular polymeric substances in membrane biofouling layers," *Environ. Sci. Technol.*, vol. 40, no. 21, pp. 6642–6646, 2006.

[20] Z. Xue, H. Lu, and W. T. Liu, "Membrane biofouling characterization: Effects of sample preparation procedures on biofilm structure and the microbial community," *Biofouling*, vol. 30, no. 7, pp. 813–821, 2014.

[21] "45359 Epoxy-Embedding Kit Product Information." Sigma-Aldrich, St. Louis, MO, 2015.

[22] J. Schindelin *et al.*, "Fiji: An open-source platform for biological-image analysis," *Nat. Methods*, vol. 9, no. 7, pp. 676–682, 2012.

[23] T. Collier, M. Follen, A. Malpica, and R. Richards-Kortum, “Sources of scattering in cervical tissue: determination of the scattering coefficient by confocal microscopy,” *Appl. Opt.*, vol. 44, no. 11, pp. 2072–2081, 2005.

[24] T. R. Garrett, M. Bhakoo, and Z. Zhang, “Bacterial adhesion and biofilms on surfaces,” *Prog. Nat. Sci.*, vol. 18, no. 9, pp. 1049–1056, 2008.

[25] S. M. Kerry *et al.*, “The intracluster correlation coefficient in cluster randomisation.,” *BMJ (Clinical research ed.)*, vol. 316, no. 7142. p. 1455, 1998.

Appendix A. Statistical Tests for Biofouling Thickness

Figure 9 shows the means, standard deviations, and results of the two-sample t-tests for means for protein and polysaccharide relative biofouling thicknesses between embedded and optical sections. Relative biofouling thickness was calculated as described in Equation 1 (section 3.7). The results of the t-tests (Prob > |t| is less than 0.05) both suggested to reject the null hypothesis that there is not a significant difference between the mean protein/polysaccharide relative biofouling thicknesses for embedded and optical sections.

A

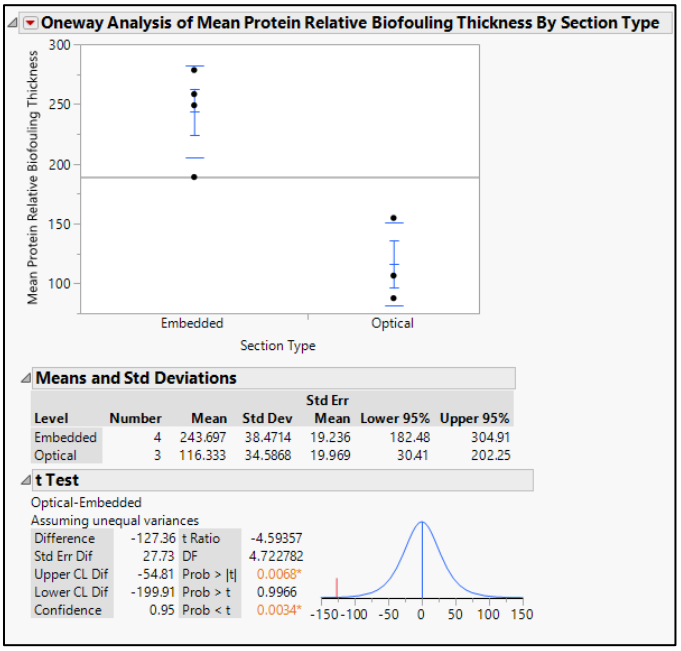

B

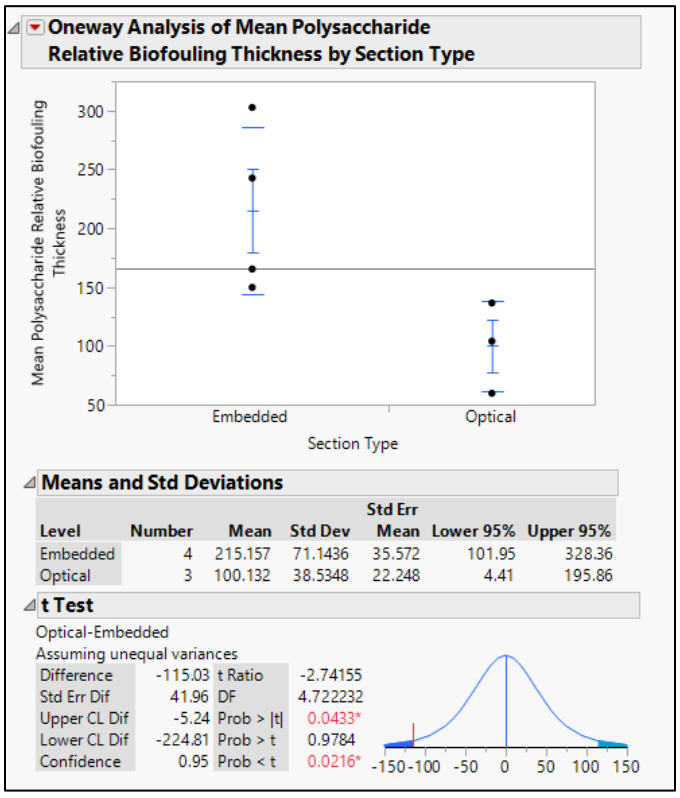

Figure 9: Statistical analysis tests for mean (A) protein and (B) polysaccharide relative biofouling thickness comparisons between embedded and optically-sectioned membranes.

Figure 10 shows the means, standard deviations, and results of the two-sample t-tests for means for protein and polysaccharide unscaled biofouling thickness between sonication treatments for embedded membranes. The results of the t-test (Prob > |t| is less than 0.05) for 10A suggested to reject the null hypothesis that there is not a significant difference between the mean protein biofouling thickness for sonication treatments of embedded membranes. However, the results of the t-test (Prob > |t| is greater than 0.05) for 10B suggested not to reject the null hypothesis that there is not a significant difference between the mean polysaccharide biofouling thickness for sonication treatments of embedded membranes.

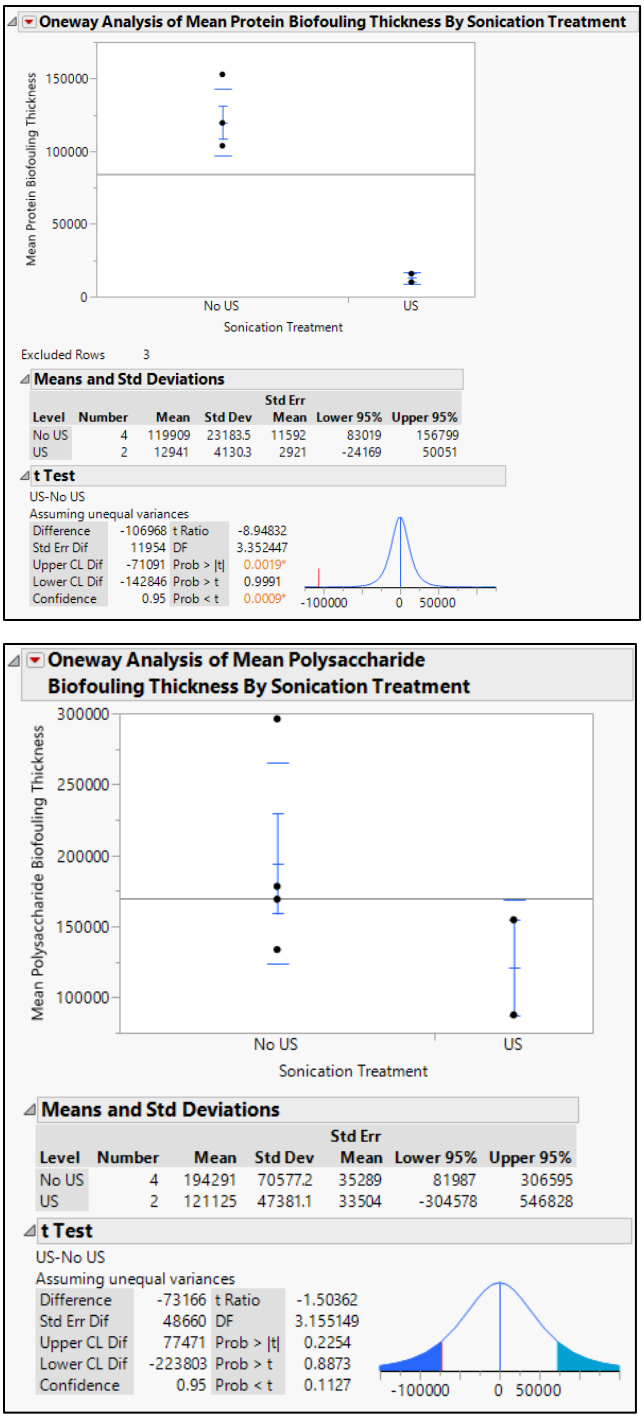

Figure 10: Statistical analysis tests for mean (A) protein and (B) polysaccharide biofouling thickness comparisons between sonication treatments of embedded membranes.

Appendix B. Mean Biofouling Depth Data

Table 2: Mean membrane biofouling total depth measurements

Treatment Type and Total Sample Number (N)	**Mean Biofouling Depth (μm)**	**Standard Deviation (μm)**
Embedded – No Sonication, N = 4	433.029	101.955
Optically-Sectioned – No Sonication, N = 3	288.8	140.129
Embedded – Sonication, N = 2	130.711	65.514

Appendix C: Wastewater Storage Reactor Quality Measurements

Table 3: Wastewater storage reactor quality measurements during testing period

Day	Date	pH	Conductivity (µS/cm)	TOC (mg Carbon/L)	TN (mg Nitrogen/L)	Total Suspended Solids (mg/L)	Volatile Suspended Solids (mg/L)	DO (mg/L)
1	4/30/2018	6.94	931	48.37	6.382	1945	1596	4.98
2	5/1/2018	6.88	966	x	x	x	x	6.87
3	5/2/2018	6.85	970	x	x	x	x	3.91
4	5/3/2018	6.9	975	58.79	7.759	1832	1517	4.61
5	5/4/2018	6.97	1010	x	x	x	x	3.39
6	5/5/2018	7.02	995	x	x	x	x	x
7	5/6/2018	6.89	1027	66.41	11.04	1919	1584	4.26
8	5/7/2018	6.97	1018	x	x	x	x	x
9	5/8/2018	7.08	1023	x	x	x	x	2.54
10	5/9/2018	6.9	1052	71.45	13.02	1897	1569	2.34
11	5/10/2018	7.05	1040	x	x	x	x	1.23
12	5/11/2018	7.1	1059	x	x	x	x	1.52
13	5/12/2018	7.02	1058	68.67	15.08	1932	1589	3.31
14	5/13/2018	7.05	1077	x	x	x	x	3.43
15	5/14/2018	7.1	1051	x	x	x	x	2.48
16	5/15/2018	6.95	1082	75.04	18.15	1872	1560	0.52
17	5/16/2018	7.19	1061	x	x	x	x	2.62
18	5/17/2018	7.22	1064	x	x	x	x	4.68
19	5/18/2018	7.14	1099	x	x	1859	1523	3.21
20	5/19/2018	7.27	1093	x	x	x	x	10.01
21	5/20/2018	7.19	1107	x	x	x	x	4.65